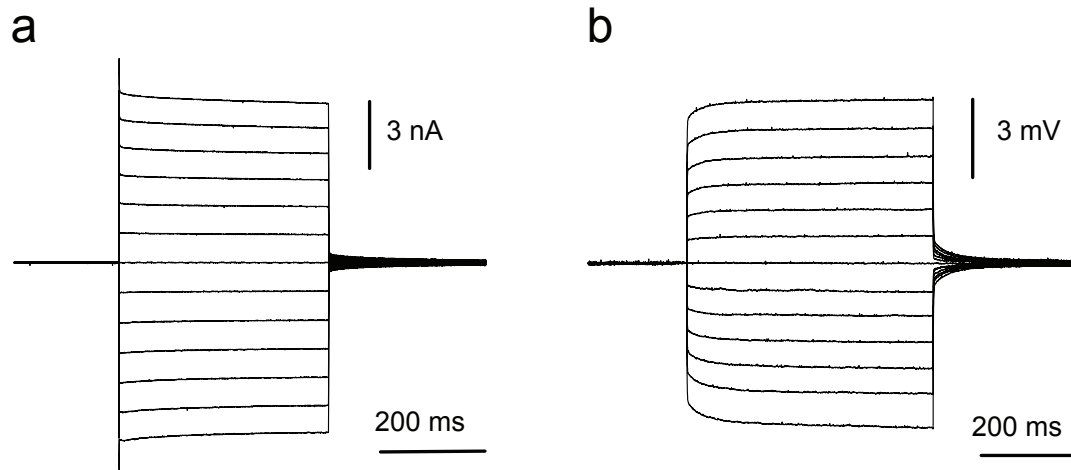
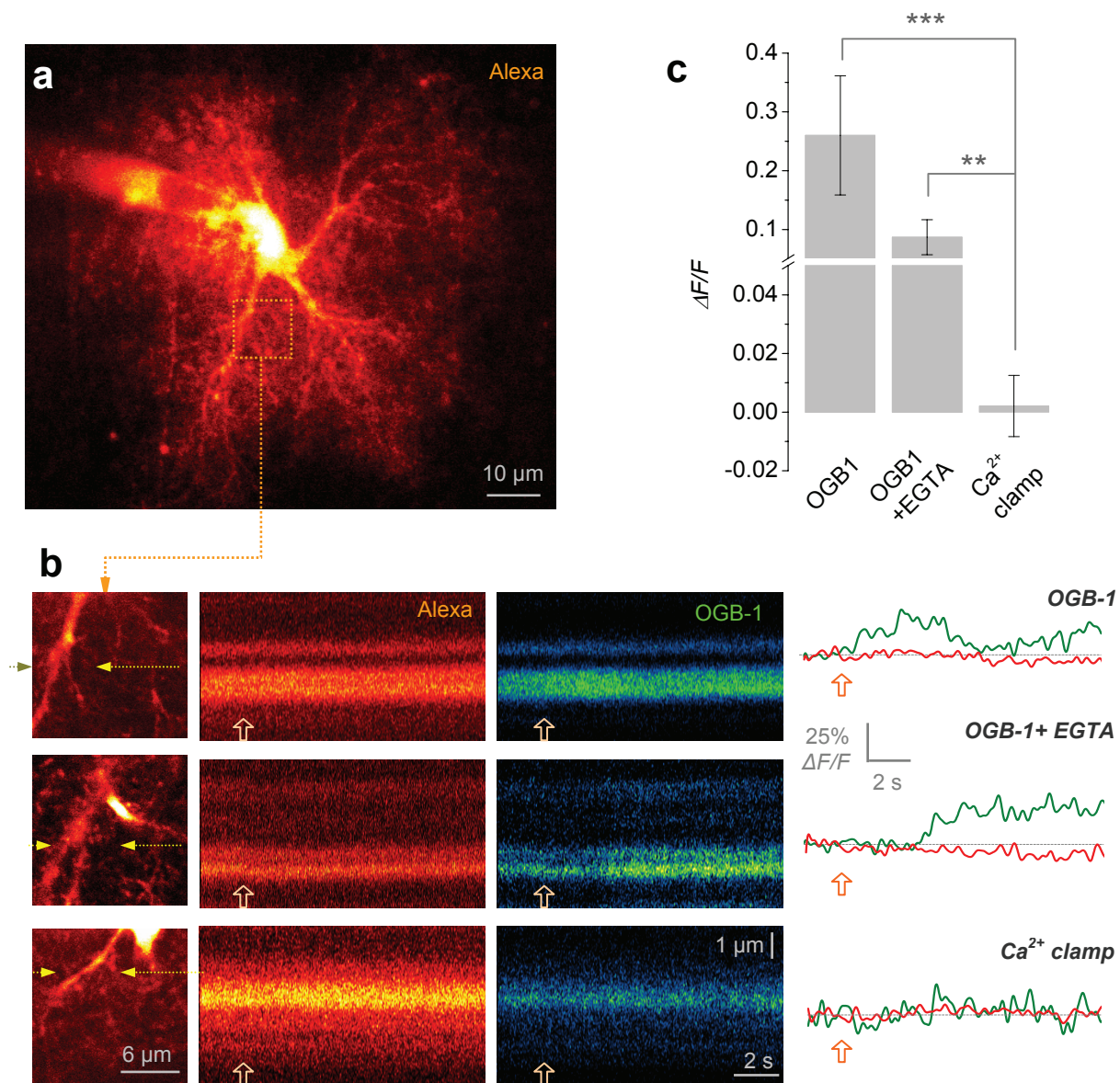


SUPPLEMENTARY INFORMATION

**Supplementary Figure 1. Ohmic properties of passive astrocytes in hippocampal area CA1.**

a-b, Electric responses of a *stratum radiatum* astrocyte held in whole-cell mode, to a square pulse of holding voltage (**a**, 10 mV steps shown) or current (**b**, 100 pA steps shown) in voltage- or current-clamp mode, respectively.



Supplementary Figure 2. Evoked intracellular Ca^{2+} transients in astrocytes are suppressed by Ca^{2+} clamp but not by Ca^{2+} buffers alone.

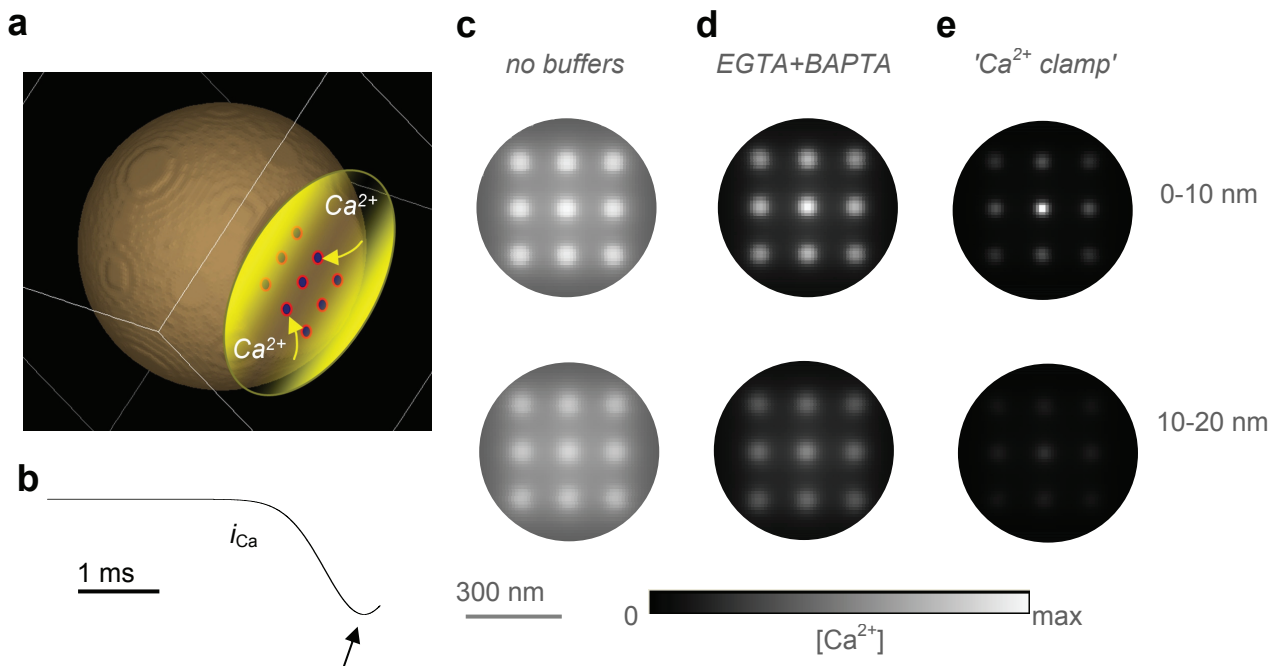
a, A characteristic example of a CA1 astrocyte held in whole-cell mode (averaged 31-image z-stack, Alexa channel, $\lambda_{\text{ex}}^{2\text{p}} = 800 \text{ nm}$) and loaded with the control intracellular solution including 200 μM Oregon Green BAPTA-1 (OGB-1, Methods). Dotted square: a selected region-of-interest (ROI) for Ca^{2+} imaging in secondary processes, as detailed in **b**.

b, Examples of Ca^{2+} -dependent fluorescence transients monitored in processes of individual astrocytes following HFS of Schaffer collaterals (1 s at 100 Hz, truncated LTP induction protocol) in control conditions of exogenous Ca^{2+} buffering (upper row; 200 μM OGB-1), under the EGTA protocol (middle row; 200 μM OGB-1 and 450 μM EGTA; OGB-1+EGTA) and under the Ca^{2+} -

clamp protocol (bottom row; OGB-1, 450 μM EGTA and 140 μM CaCl_2 ; Ca^{2+} -clamp). The protocols were selected so that the only difference between *OGB-1+EGTA* and Ca^{2+} -clamp was the presence of exogenous Ca^{2+} , to ensure that fluorescence imaging conditions and Ca^{2+} buffers were matched between the two protocols. Left panels, typical astrocyte fragments selected for Ca^{2+} imaging (upper panel depicts a single-section fragment from the astrocyte shown in **a**, as indicated; other full-astrocyte images are not shown; scale bar applies throughout). Middle panels, the respective linescan traces recorded simultaneously in the Alexa (Ca^{2+} insensitive) and OGB-1 (Ca^{2+} sensitive) channels; block arrows, HFS stimulation; false colour tables are used; scale bars apply throughout. Right panels, the corresponding digitised line scan traces depicting Ca^{2+} signals (OGB-1, green) against Ca^{2+} -insensitive fluctuations (Alexa, red), as indicated; signals were normalised against the baseline and corrected for background fluorescence; a slight signal decrease in the red channel reflects residual photobleaching of Alexa; pixel noise was suppressed using a low-pass Fourier filter (cut-off frequency 50 Hz); scale bars apply throughout. Note that the waveforms of HFS-evoked Ca^{2+} fluorescence transients recorded in cell processes were non-uniform often including repetitive events lasting for several seconds, which was consistent with earlier observations¹.

A note on sampling: Because in these experiments the imaging of transient Ca^{2+} signals in the soma or proximal primary dendrites could be compromised by the interfering presence of the dialysing pipette, ROI sampling was quasi-random: fragments of astrocyte processes occurring 10-20 μm from the soma in three dimensions, against a relatively clear background (in single optical sections) were selected arbitrarily, with no visual preferences. One fragment per cell was imaged in a single experiment, to ensure the continuity of baseline (pre-LTP) conditions.

c, Statistical summary of experiments illustrated in **a-b**. Bars, average values; error bars, s.e.m.; $\Delta F/F$, the evoked fluorescence response in the OGB-1 (green) channel: $\Delta F/F = (F_1 - F_0)/F_0$ where indexes 0 and 1 represent the linescan intensity averaged, respectively, 400 ms before and 2 s after the stimulation onset (sampling window centred on the peak fluorescence response), with background fluorescence subtracted and focus fluctuations corrected using the Alexa (red) channel; photobleaching in the green channel was negligible. The average values in the three cases were, respectively: $26 \pm 10\%$ ($n = 6$; *OGB-1*); $8.7 \pm 3.0\%$ ($n = 8$; *OGB1 + EGTA*), and $0.21 \pm 0.10\%$ ($n = 12$; Ca^{2+} clamp). ***, $p = 0.0022$; **, $p = 0.0059$ (unpaired t -tests).



Supplementary Figure 3. Clamping intracellular Ca^{2+} is more efficient than Ca^{2+} buffers alone in restricting the spatial extent of Ca^{2+} nanodomains near Ca^{2+} sources.

a, A 3-D model of a cell cytoplasm fragment (in beige; diameter 1 μm , 0.2 μm segment truncated) adjacent to a putative Ca^{2+} source (yellow) which is equipped with Ca^{2+} channels (nine 50 nm channel clusters depicted by dots).

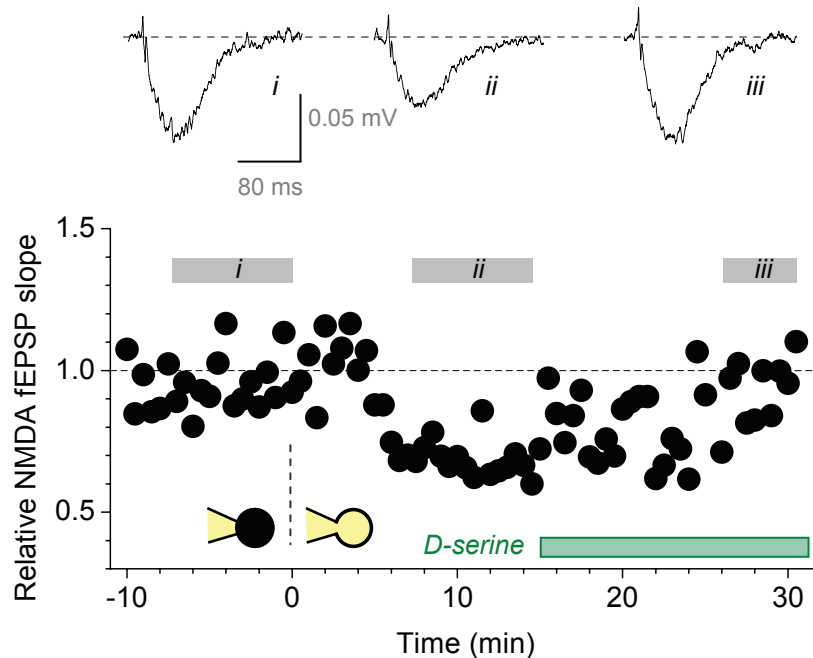
b, Ca^{2+} entry time course, with a rapid rise characteristic of Ca^{2+} channel opening. The shape of Ca^{2+} nanodomains is analysed at the current peak (arrow), which corresponds to ~ 1100 Ca^{2+} ions entered through each channel cluster². Varying the cytoplasm geometry, the size of channel clusters or Ca^{2+} current had little impact on the qualitative conclusion of these simulations.

c, A snapshot depicting the simulated 3-D concentration profile of free intracellular Ca^{2+} (nanodomains), at the peak of Ca^{2+} entry, in the sub-membrane layers immediately adjacent to the Ca^{2+} sources (upper and lower panels, 0-10 nm and 10-20 nm from the membrane, respectively). Grey levels represent relative concentrations, on the scale from zero to the maximum level (inside the nanodomain). The cell cytosol contains no Ca^{2+} buffers.

d, A Ca^{2+} concentration snapshot as in **c**, but with the cell cytosol containing 0.45 mM free EGTA, 0.2 mM free OGB-1, and $\sim 0.1 \mu\text{M}$ free Ca^{2+} as initial conditions (the non-equilibrium may reflect highly localised sources and active removal of free Ca^{2+} from the system).

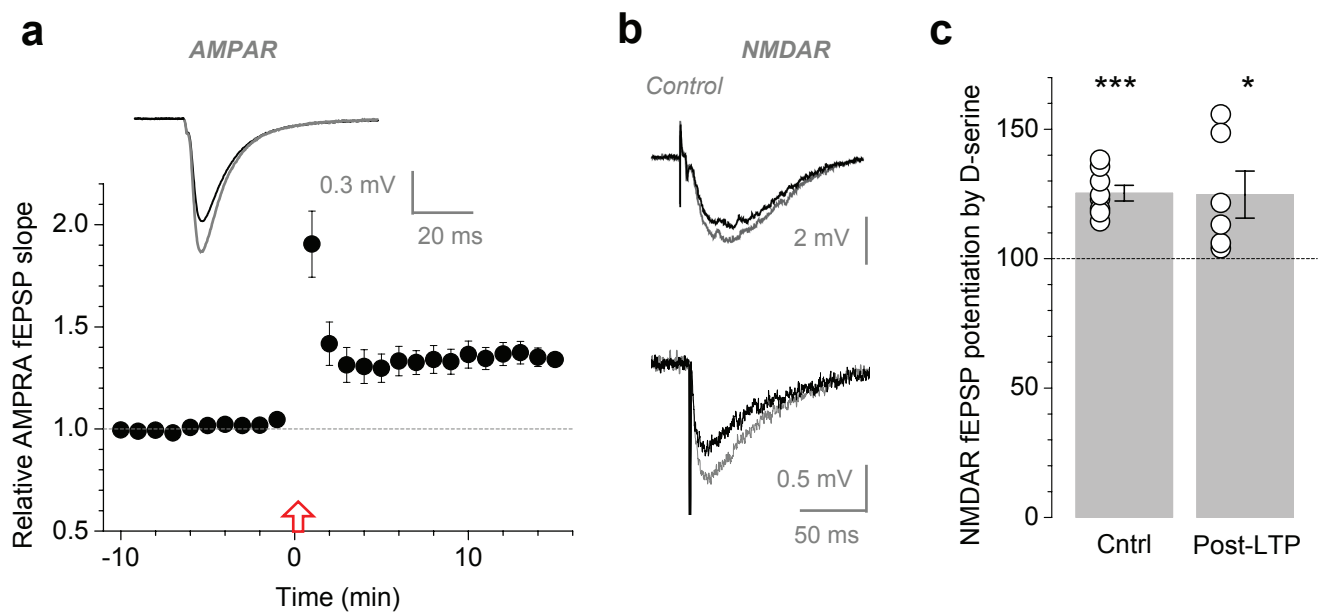
e, A Ca^{2+} concentration snapshot as in **c-d**, but with the cell cytosol containing 0.45 mM total EGTA, 0.2 mM total OGB-1 and 0.14 mM total Ca^{2+} equilibrated yielding (in mM): ~ 0.37 free / 0.08 bound EGTA, ~ 0.13 free / 0.07 bound OGB-1, and ~ 0.0001 free / 0.14 bound Ca^{2+} reflecting the Ca^{2+} clamp conditions used in our experiments.

Modelling. Simulations were carried out using *Virtual Cell* (VCell), version 4.5 at the National Resource for Analysis and Modeling (NRAM), NIH, CT. Geometry, boundary conditions and binding reaction parameters with Ca^{2+} buffers were as detailed previously³. The compartment size was $10 \times 10 \times 10 \text{ nm}^3$ giving a total of $1.21 \cdot 10^6$ compartments; time step, 50 μs .



Supplementary Figure 4. A one-cell example of the experiment illustrated in Fig. 2a, with Ca^{2+} clamp solution in the patched astrocyte.

Astrocyte whole-cell break-in is shown by a vertical dotted line; dots, individual NMDAR fEPSP slope values; traces, fEPSPs averaged over the experiment epochs depicted by the corresponding Roman numerals. Other notation is as in Fig. 2a (main text).

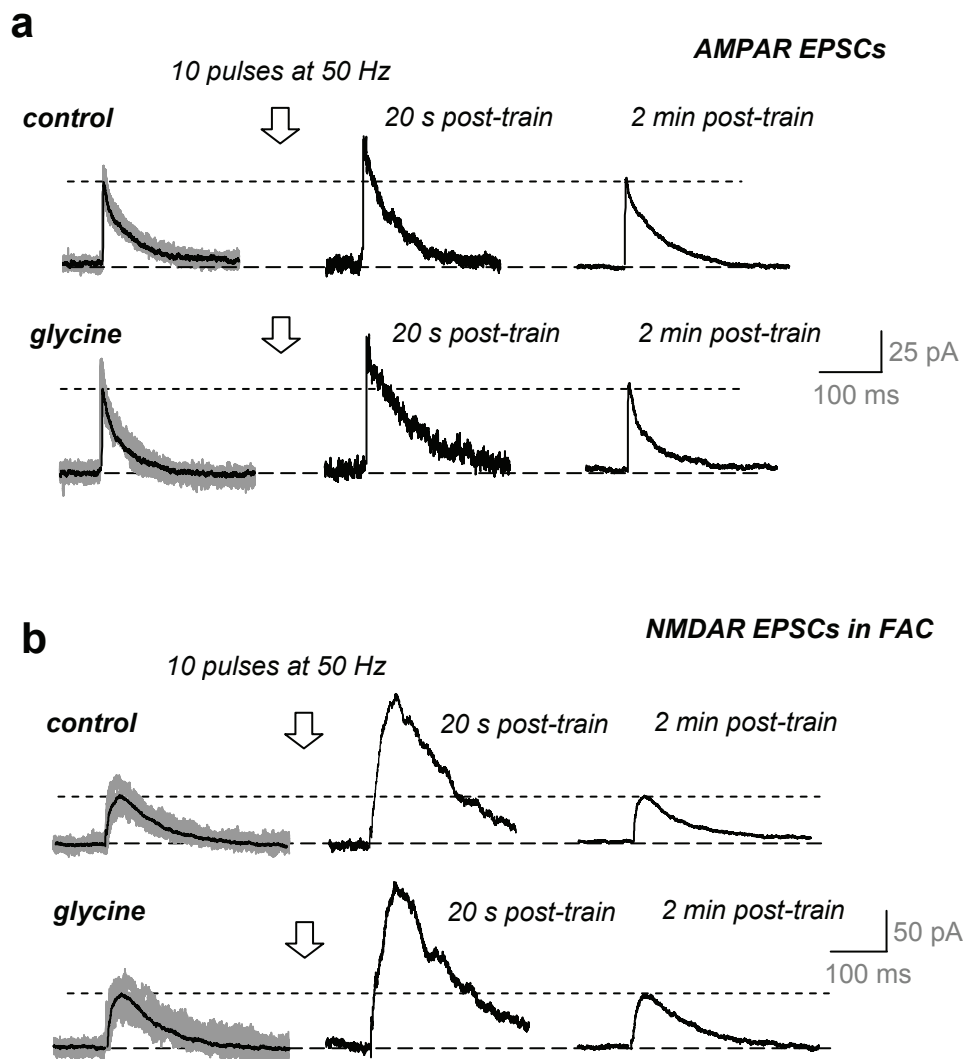


Supplementary Figure 5. LTP has no long term effect on the NMDAR glycine site occupancy.

a, In each test trial, LTP of AMPAR fEPSPs was induced using the HFS protocol (Methods; average potentiation $136 \pm 6\%$, $n = 6$). Once the persistence of potentiation was established, $10 \mu\text{M}$ NBQX was added to the bath to monitor the NMDAR-dependent response component (see **b**).

b, Traces show characteristic NMDAR fEPSPs before and after application of D-serine (black and grey, respectively) in control conditions and post-LTP (stimulation strength unchanged, $10 \mu\text{M}$ NBQX and 1.3 Mg^{2+} throughout), as indicated.

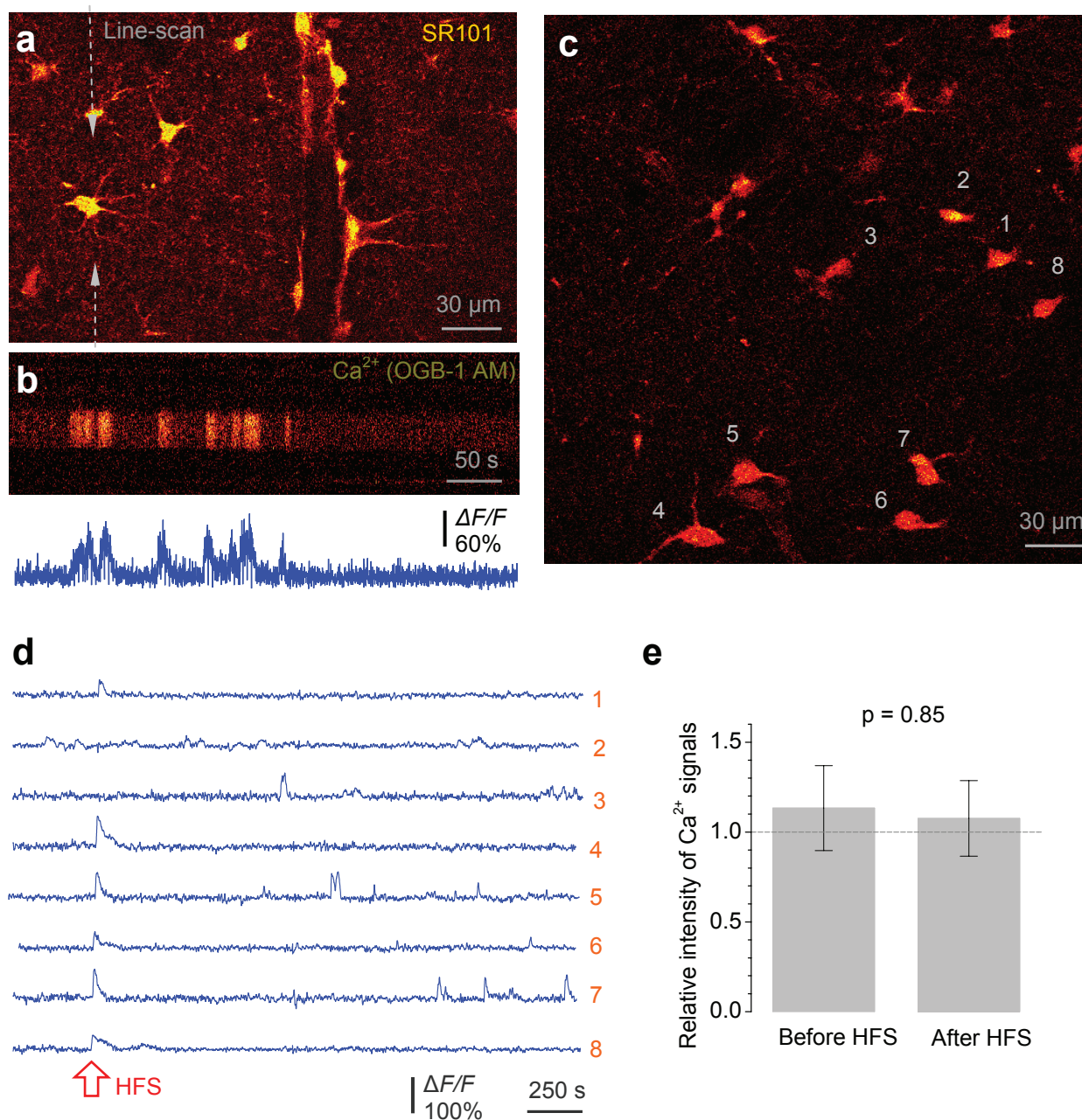
c, Statistical summary: D-serine ($10 \mu\text{M}$) potentiates NMDA fEPSPs in control conditions by $25.3 \pm 3.0\%$ (*Cntrl*; $n = 8$, $p < 0.0001$) and inducing LTP has no effect on this increase (*Post-LTP*; average increase, $24.7 \pm 9.1\%$, $n = 6$, $p = 0.042$; difference with control conditions at $p = 0.946$); bars, mean \pm s.e.m.; circles, individual experiments. These data are fully consistent with the results of whole-cell recordings in CA1 pyramidal cells (Fig. 2c of the main text) suggesting that the average occupancy level of the NMDAR co-agonist site is not affected by LTP.



Supplementary Figure 6. The transient potentiation of AMPAR EPSCs, or NMDAR EPSCs in the presence of FAC, evoked by repetitive stimuli is insensitive to glycine (addendum to Fig. 3d, main text).

a, Examples of AMPAR EPSCs evoked in one cell by a single stimulus in baseline conditions (left: grey lines, individual traces; black, average), 20 seconds after the train of 10 stimuli at 50 Hz (middle: as indicated), and 2 min after the train (right), in control (upper row) and in the presence of 0.1 mM glycine (lower row); $V_m = +40$ mV in the presence of 50 μ M APV.

b, Examples of EPSCs including a prominent NMDAR component (NMDAR EPSCs) recorded in the presence of 5 mM FAC (>60 min) in experiments similar to those in **a**, as indicated. Relative changes in the NMDAR-mediated currents were measured as the charge (area under the EPSC) measured over the 100-300 ms post-peak interval.



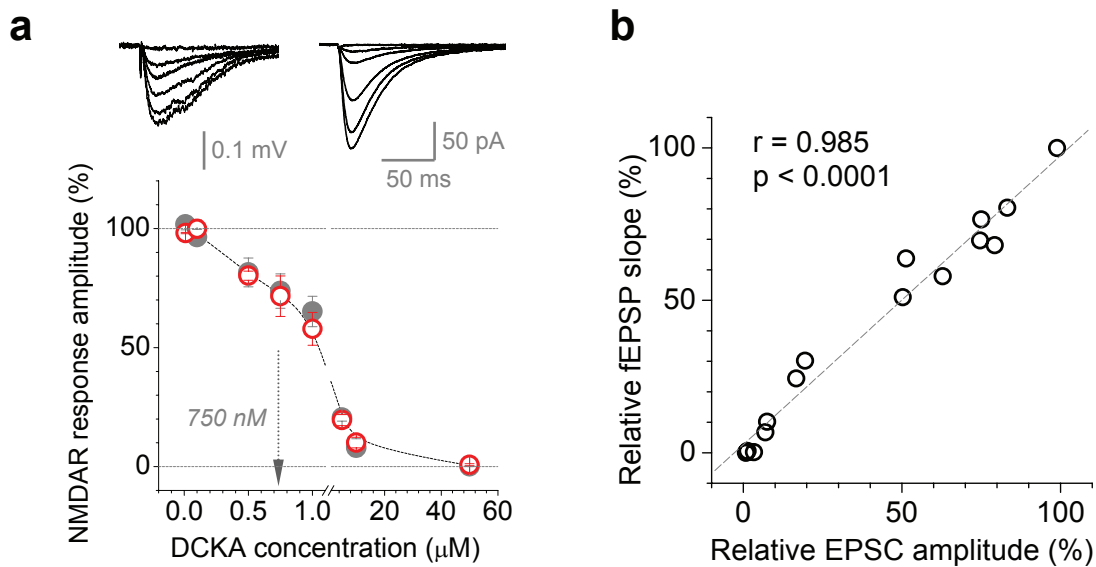
Supplementary Figure 7. The LTP induction protocol (HFS) induces somatic Ca²⁺ elevations in many astrocytes but has no lasting effect on the average rate of spontaneous astrocytic Ca²⁺ signalling.

a, A characteristic view of CA1 astrocytes labelled with sulforhodamine 101 (SR101; $\lambda_x^{2P} = 800 \text{ nm}$; Methods) imaged in a single focal plane $\sim 100 \mu\text{m}$ deep in the slice. A blood vessel profile is seen, with the adjacent astrocyte endfeet. Arrows, a linescan position for Ca²⁺ imaging in a selected cell.

b, An example of spontaneous Ca^{2+} activity monitored in the astrocyte depicted in **a** (OGB-1 excitation at $\lambda_{\text{x}}^{2\text{P}} = 800 \text{ nm}$). Upper and lower panel, linescan image and the corresponding trace, respectively. In some experiments, Fluo-4 AM was used for Ca^{2+} imaging.

c-d, A typical sample of CA1 astrocytes (**c**) to monitor Ca^{2+} during the application of HFS to Schaffer collaterals (LTP-induction protocol, onset indicated by the red arrow in **d**). Simultaneous monitoring of multiple astrocytes was carried out in frame-scan mode at either 2 or 7 Hz and the corresponding image resolution (256 x 256 or 64 x 64 pixels, respectively). In each experiment, image series consisting of 800-20000 frames were collected. Ca^{2+} -dependent fluorescence emission was measured using individual regions-of-interests representing astrocytic somata. Numerals in **c** and **d** indicate examples of the corresponding recorded cells. 20 out of 37 recorded astrocytes (~54%) responded to HFS with a slow, clearly detectable Ca^{2+} elevation (exemplified by cells 1, 4, 5, 6, 7, 8 in **d**; note that volume-integrated Ca^{2+} imaging might conceal non-uniform Ca^{2+} signalling events detectable at higher resolution in individual astrocytic fragments).

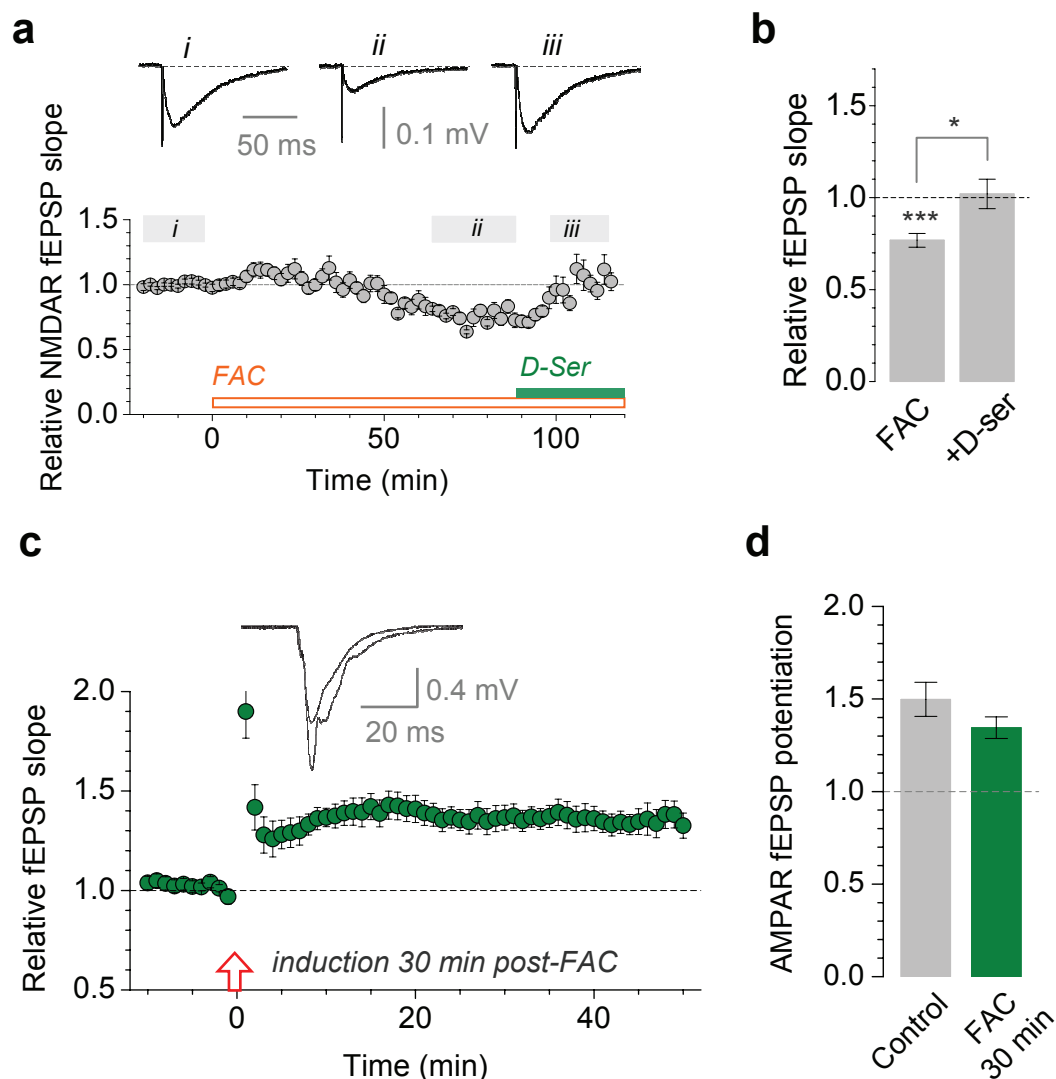
e, HFS does not affect the average intensity of spontaneous Ca^{2+} waves in CA1 astrocytes. The average strength W of spontaneous Ca^{2+} elevations - a measure combining the amplitude and frequency / duration of events in an astrocyte - was calculated as the fraction of recording time during which Ca^{2+} -dependent fluorescence was >50% above the baseline. The global mean W across the sample was $5.2 \pm 1.2\%$ (mean \pm s.e.m.; $n = 37$). To account for any time-dependent trend in the recorded fluorescence (e.g., due to photobleaching or dye extrusion), in each i th astrocyte we related its W_i value to the average control value W_c averaged among astrocytes in control slices (no HFS exposure) over the same recording intervals, with the matched timing post-dye loading (control pool, $n = 18$ cells). Bar graph, W_i / W_c (mean \pm s.e.m.) before and after HFS application.



Supplementary Figure 8. The selective NMDAR co-agonist site blocker DCKA reduces NMDAR responses (both EPSCs and fEPSPs) by ~25% at a concentration of 750 nM.

a, A dose-response curve of DCKA obtained by recording either NMDAR fEPSPs (open circles) or whole-cell NMDAR EPSCs (grey circles) evoked by stimulation of Schaffer collaterals; individual circles correspond to $n = 2-8$. Traces, characteristic fEPSPs (left) and EPSCs (right) recorded in one cell in baseline conditions and at 500 nM, 1 μM, 5 μM, 10 μM and 50 μM DCKA, correspondingly. Grey arrow, DCKA concentration (~750 nM) at which the NMDAR responses are suppressed by ~25%, thus mimicking the effect of the astrocytic Ca^{2+} clamp (Fig. 2a-b of the main text).

b, A summary of experiments in which NMDAR EPSCs and fEPSPs were recorded simultaneously at different concentrations of DCKA ($n = 15$); dotted line, linear regression; r , correlation coefficient.



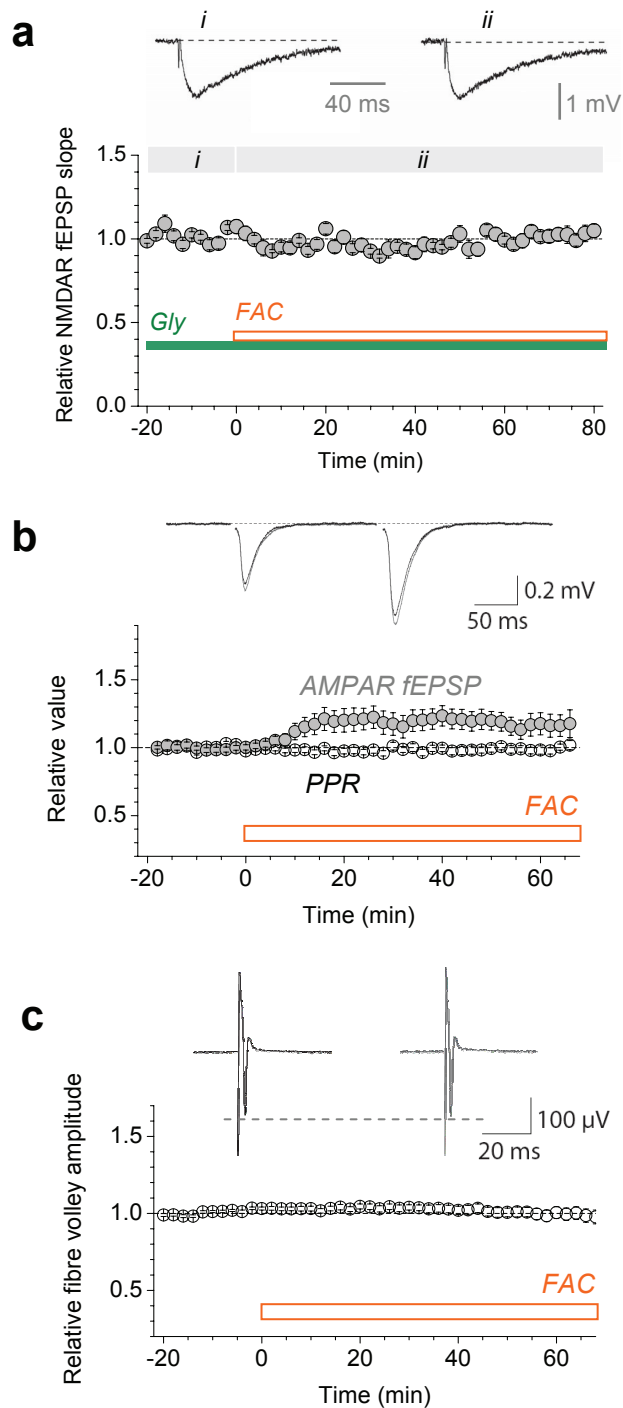
Supplementary Figure 9. FACS reduces NMDA fEPSPs 40-50 min after application and has no effect on LTP before that time (Fig. 3d).

a, The amplitude of NMDAR fEPSPs monitored during the application of 5 mM fluoroacetate (FAC) and, subsequently, 10 μ M D-serine ($n = 16$), as shown (mean \pm s.e.m.). Traces, fEPSPs averaged over the recording epochs, as indicated.

b, Statistical summary of experiments shown in **a**. Bars, mean \pm s.e.m. relative to baseline; *, $p = 0.0127$; ***, $p < 0.001$ (two-population t -test).

c, Time course of the average AMPAR fEPSP slope (mean \pm s.e.m.) following 30 min incubation with 5 μ M FAC.

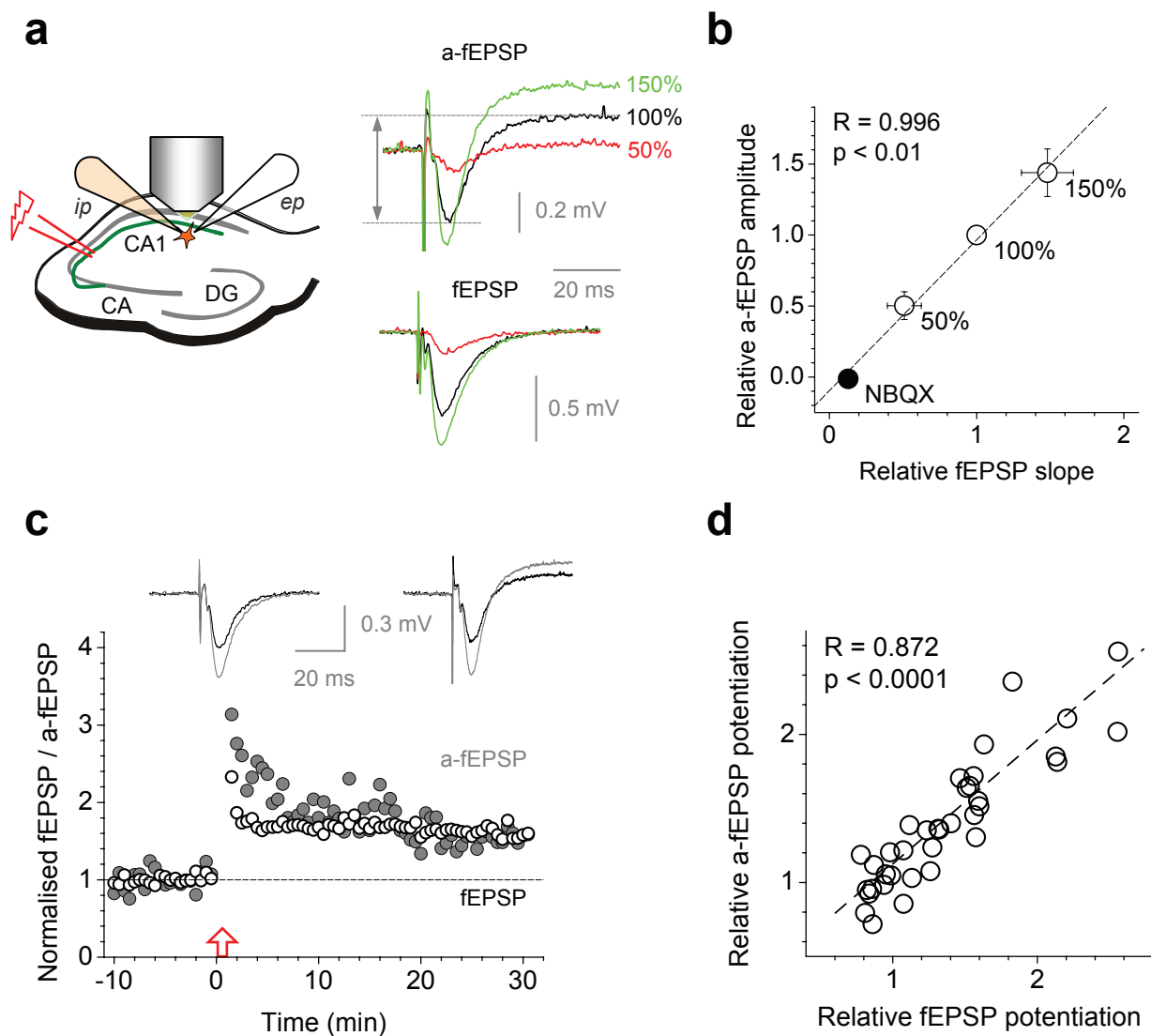
d, Statistical summary of experiments depicted in **c** also showing LTP in control conditions. Average potentiation in FAC was 34.5 ± 5.8 % (n = 12, p = 0.134 compared to control LTP).



Supplementary Figure 10. Effects of FAC on excitatory responses.

a, Application of 5 mM FAC in the presence of 0.1 mM glycine had no effect on NMDAR fEPSPs (average change $2.3 \pm 4.2\%$, $n = 6$). Traces, characteristic NMDAR fEPSPs averaged over the experimental epochs depicted by grey segments *i* and *ii*, correspondingly; one cell example.

b-c, FAC slightly increases AMPAR-mediated fEPSPs (**b**, grey circles; average increase: $18.6 \pm 6.9\%$, $n = 17$, $p = 0.008$) which might reflect increased postsynaptic excitability in the absence of glutamate uptake. At the same time, FAC had no effect on the afferent fibre volley (**c**; average change $-1.0 \pm 3.8\%$, $n = 20$, $p = 0.460$) or the paired-pulse ratio (**b**, open circles; average change: $0.0 \pm 1.9\%$, $n = 13$, $p = 0.864$) indicating that axonal excitability or release probability were not affected by FAC. Traces in **b**, characteristic paired-pulse AMPAR EPSPs in baseline conditions and after application of FAC (black and grey lines, respectively); traces in **c**, characteristic fibre volley recordings (in $10\ \mu\text{M}$ NBQX, $50\ \mu\text{M}$ AP-5 and $50\ \mu\text{M}$ picrotoxin) before and after application of FAC (left and right, respectively).



Supplementary Figure 11. Recording field EPSPs through a passive astrocyte in whole-cell mode.

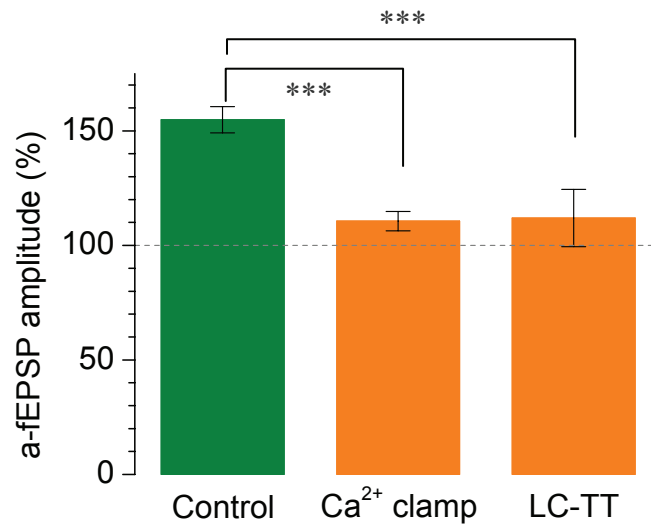
a, Diagram, experimental arrangement: stimuli are applied to Schaffer collaterals through a bipolar extracellular stimulating electrode (shown), and responses are recorded both through an extracellular glass electrode and a whole-cell patch pipette through the astrocyte, as depicted. Due to their low input resistance ($8.4 \pm 0.6 \text{ M}\Omega$, mean \pm s.e.m., $n = 146$) and ohmic properties (Supplementary Fig. 1), astrocyte responses to afferent stimulation contain a relatively fast component reflecting field potentials generated in the adjacent neuropil. Traces, electrical responses of a passive astrocyte held in current-clamp mode (a-fEPSP, upper panel) and simultaneously recorded local fEPSPs (lower

panel) at three stimulus strength values, as indicated. Although the glial transporter current can be routinely dissociated from a-fEPSPs, e.g., using kynurenate⁴, we left the transporters intact: firstly, to ensure the pharmacological compatibility with other experiments, and, secondly, because the compound a-fEPSP amplitude (the maximum range of the field potential transient, as depicted by arrow) correlated tightly with the fEPSP slope (shown below in **b** and **d**).

b, Statistical summary of experiments depicted in **a**, for $n = 4$ slices (dots and error bars show mean \pm s.e.m.). The data indicate that the a-fEPSP amplitude (as shown in **a**) is tightly correlated with the fEPSP slope across the sample, with no detectable bias from the components representing glutamate transporter current or potassium conductance^{4,5}; R , coefficient of correlation.

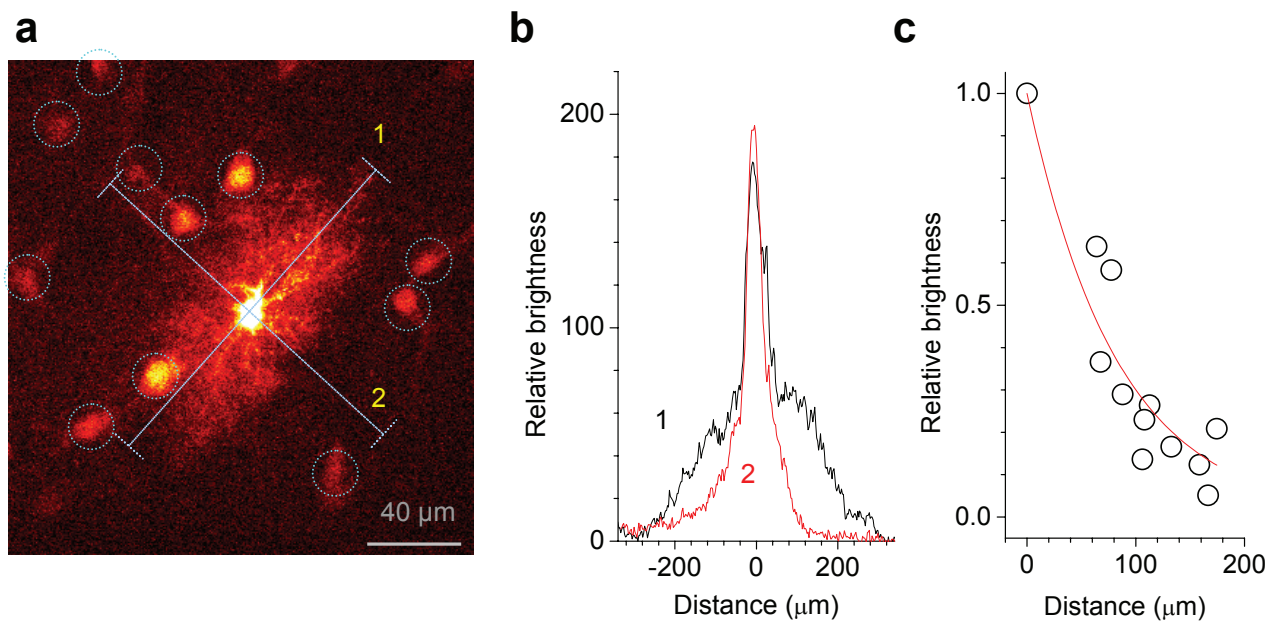
c, A one-cell example showing that the degree of LTP could be reliably monitored using either the slope of fEPSP in *stratum radiatum* or the a-fEPSP amplitude (hollow and grey circles, respectively). High-frequency stimuli (three trains of 100 pulses at 100 Hz, 60 s apart) were applied at time point zero (red arrow).

d, Statistical summary of experiments depicted in **c** ($n = 37$ slices). Dots, the extent of LTP expression in individual experiments relative to baseline, measured using the fEPSP slope (abscissa) and the a-fEPSP amplitude (ordinate; all individual slices are shown including those showing insignificant LTP). A tight correlation between the two measures is evident; notation is the same as in **b**.



Supplementary Figure 12. A summary of experiments in which LTP of a-fEPSPs was monitored in different experimental conditions.

All recordings were pooled into groups according to the composition of the intracellular solution used: *control* solution ($n = 30$), *Ca²⁺ clamp* (0.45 mM EGTA, 0.2 mM OGB-1 and 0.14 mM CaCl₂ added; $n = 23$), and LC-TT (1 μ M light chain tetanus toxin added; $n = 14$). The data represent experiments with one or two astrocytes patched (see Fig. 4). Bars, the average a-fEPSP amplitude relative to baseline; error bars, s.e.m.; ***, $p < 0.0001$ (two-population t -test).



Supplementary Figure 13. Assessing the spatial extent of astrocytic arbours and the diffuse spread of Alexa dye through gap junctions.

a, A characteristic fluorescence image of a CA1 astrocyte loaded in whole-cell mode with Alexa Fluor 594 (40 μM; $\lambda_{ex}^{2P} = 800$ nm); average projection is shown for a ~100 μm deep stack corrected for the apparent decay of excitation-emission with depth (an average decay length constant, ~41 μm, was obtained in separate experiments); also depicted in Fig. 5h. The spatial extent of an individual astrocyte arbour is evaluated by measuring fuzzy fluorescence profiles sampled as illustrated by segments 1 and 2. Significant diffusion escape of the dye through gap junctions is evident from clearly stained neighbouring astrocytic somata (dotted circles). Because ~1 μm thick optical sections through such somata include no extracellular space, their fluorescence signal can be used to gauge the spatial profile of dye diffusion escaping from the patched cell (in the middle) through gap junctions.

b, Fluorescence emission profiles (examples) representing the astrocytic arbour taken as depicted by arrows in **a**.

c, Relative fluorescence recorded inside neighbouring astrocytic somata ($n = 11$) at different 3-D distances from the patched soma, as depicted in **a** (circles); red line, a single-exponent approximation of the fluorescence decay in the example sample shown in **a** (distance zero represents the patched astrocyte soma).

To gauge the average escape of Alexa fluorescence from a patched astrocyte through gap junctions into neighbouring cells (Fig. 4h of the main text), we used the convolution of the average profiles illustrated in **b** and **c**.

References

1. Pasti, L., Volterra, A., Pozzan, T. & Carmignoto, G. Intracellular calcium oscillations in astrocytes: a highly plastic, bidirectional form of communication between neurons and astrocytes in situ. *J Neurosci* **17**, 7817-30 (1997).
2. Koester, H. J. & Sakmann, B. Calcium dynamics associated with action potentials in single nerve terminals of pyramidal cells in layer 2/3 of the young rat neocortex. *J Physiol* **529**, 625-646 (2000).
3. Scott, R., Ruiz, A., Henneberger, C., Kullmann, D. M. & Rusakov, D. A. Analog modulation of mossy fiber transmission is uncoupled from changes in presynaptic Ca^{2+} . *J Neurosci* **28**, 7765-73 (2008).
4. Diamond, J. S., Bergles, D. E. & Jahr, C. E. Glutamate release monitored with astrocyte transporter currents during LTP. *Neuron* **21**, 425-33 (1998).
5. Luscher, C., Malenka, R. C. & Nicoll, R. A. Monitoring glutamate release during LTP with glial transporter currents. *Neuron* **21**, 435-41 (1998).